Chinese Chemical Letters 35 (2024) 108734

Contents lists available at ScienceDirect

Chinese Chemical Letters

journal homepage: www.elsevier.com/locate/cclet

Asymmetric side-chain engineering of organic semiconductor for ultrasensitive gas sensing

Xiaoying Ma[a], Xiaojuan Dai[b], Lanyi Xiang[a], Jiajun Chang[a], Danfeng Zhi[a], Haozhen Zhao[a], Zhenjie Ni[a], Ye Zou[b], Xike Gao[c], Fengjiao Zhang[a,d,*]

[a] School of Chemical Sciences, University of Chinese Academy of Sciences, Beijing 100049, China
[b] Laboratory of Organic Solids, Institute of Chemistry, Chinese Academy of Sciences, Beijing 100190, China
[c] Key Laboratory of Synthetic and Self-Assembly Chemistry for Organic Functional Molecules, Shanghai Institute of Organic Chemistry, Chinese Academy of Sciences, Shanghai 200032, China
[d] Binzhou Institute of Technology, Binzhou 256606, China

ARTICLE INFO

Article history:
Received 11 May 2023
Revised 24 June 2023
Accepted 26 June 2023
Available online 28 June 2023

Keywords:
Organic thin film transistor
Asymmetric side chain
Gas sensing
Molecular stacking
Energy level manipulating

ABSTRACT

Molecular structure of organic semiconductor plays a critical role in determining the performance and functionality of organic electronic devices, by optimizing the electrical, optical and physicochemical properties. Substituted alkyl chains are fundamental units in tailering the solubility and assemblability, among which the asymmetric properties have been reported as key element for controlling the packing motifs and intrinsic charge transport. Here, we expanded the scope of molecular asymmetry dependent sensing features based on a new series of naphthalene diimides (NDI)-based derivatives substituted with a same branching alkyl chain but various linear-shaped alkyl chains (Cn-). A clear molecular stacking change, from head-to-head bilayer to head-to-tail monolayer packing model, is observed based on the features of anisotropic molecular interactions with the change in the chain length. Most importantly, a unique LUMO level shift of 0.17 eV is validated for NDI-PhC4, providing a record sensitivity up to 150% to 0.01 ppb ammonia, due to the desired molecular reactivity and device amplification properties. These results indicate that asymmetric side-chain engineering opens a route for breath healthcare.

In the past decades, electronic gas sensors have garnered increasing attention owing to their wide application prospects in environment pollution monitoring and personalized healthcare diagnoses [1–4]. Organic thin-film transistors (OTFTs), which have developed rapidly since their invention in 1986 [5], are considered as a promising candidate that exhibit special features in terms of signal transition and gated amplification functionality to external stimulates. In an OTFT based gas sensor, the current change followed by carrier concentration and/or carrier transport following doping, quenching, or dipole effect between the active layer and analytes [6–8]. To improve the sensing performance, the critical factors that must be considered are effective interactions between the analytes and devices, and device amplification properties under an electric field. Currently, organic semiconductors (OSCs) are considered to be the primary compounds capable of manipulating the abovementioned processes because carrier accumulation and transport mainly occur within the conductive layer [9–11]. Thus, driven by the rapid development of molecular design strategies and solution processable techniques [12–16], tremendous progress has been achieved in OTFT in terms of applications in electronic noses and smart systems.

In particular, there are several requirements to be fulfilled in case of OSC molecules to facilitate excellent gas sensing performance of OTFTs [17–21]: (i) well-balanced electron affinity (or electron ionization energy) that promotes charge transfer with target analytes, (ii) fine-tuned functional groups and film microstructure that contribute to large contact area and more reaction sites, (iii) high transconductance to enable efficient amplification functionality. To achieve these goals, Oh *et al.* demonstrated a strategy to enhance the sensitivity of ammonia with stable radical anion formation *via* the extension of linear-shaped perfluoroalkyl group to the π-backbone [22]. They figured out that the electron-deficient core skeleton and electron-withdrawing substituents facilitated the adsorption of Lewis base gases, inducing a current increase >1700. In addition, substituting side chain with functional groups of OSC has been proposed to modulate molecular stacking and construct sensing recognition sites for sensitive detection.

* Corresponding author at: School of Chemical Sciences, University of Chinese Academy of Sciences, Beijing 100049, China.
E-mail address: fjiaozhang@ucas.ac.cn (F. Zhang).

https://doi.org/10.1016/j.cclet.2023.108734
1001-8417/

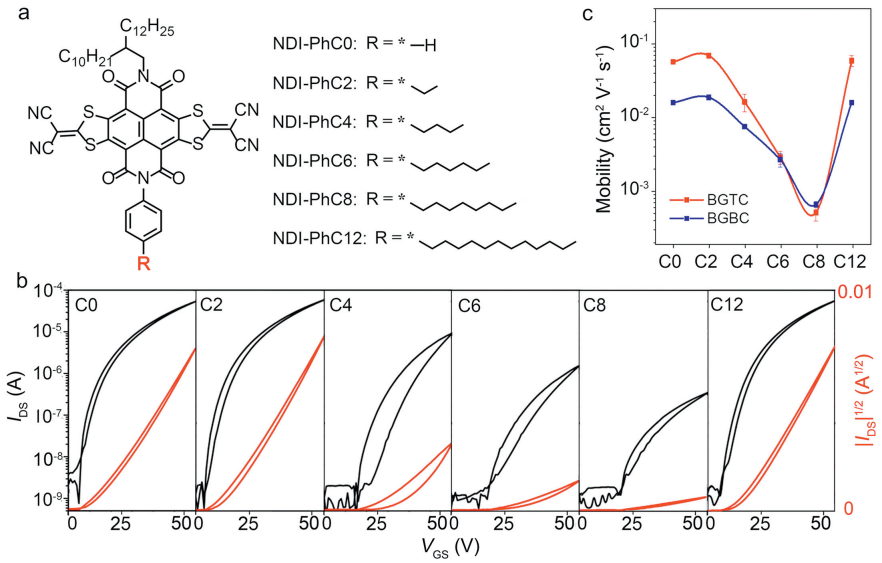

Fig. 1. (a) Molecular structures of NDI-PhC0, NDI-PhC2, NDI-PhC4, NDI-PhC6, NDI-PhC8, NDI-PhC12. (b) Transfer characteristics and (c) device mobility of BGTC OTFTs based on NDI-PhCn derivatives. All data were obtained from the optimized temperature. V_{DS} = 60 V.

For instance, Yao *et al.* reported increased ammonia sensitivity (LOD = 10 ppb) through the introduction of urea groups in diketopyrrolopyrrole (DPP)-quaterthiophene polymer [23], attributing to the high mobility and effective charge transfer *via* H-bonding formation. Recently, certain new insights have been reported in the symmetric side-chain engineering of OSC development, which facilitate a bilayer-to-monolayer stacking change [24–26]. Interestingly, the asymmetric alkyl chain enhances charge transport along the delocalized bilayer stacking models. Despite these enlightening studies, the role of molecular asymmetry in controlling the sensing performance remains unclear, due to the lack of an in-depth understanding of molecular interactions and charge transfer properties.

This study explored the effect of molecular asymmetry on ammonia sensing performance in case of naphthalene diimide derivatives (NDI-PhCn) (Fig. 1a). The NDI core was substituted with branching alkyl and phenyl-alkyl chains with different lengths. Based on electrical and morphological characterizations, we elucidated that decrease the molecular asymmetry degree of NDI-PhCn molecules facilitated the conjugated backbone transformed from head-to-head packing to head-to-tail packing. In addition, it not only tuned the mobility and provided more gas diffusion pathways, but also induced an increase in the electron affinity (a lower LUMO level). Hence, the charge transfer properties between OSC and Lewis base gas can be manipulated *via* fine-tuned redox interaction. Consequently, we obtained a maximum two orders of increase in magnitude in case of sensitivity to ammonia based on NDI-PhC4 OTFTs which is the highest response among previous reports. Thus, this investigation demonstrated that the asymmetry engineering on alkyl chain can promote a method of device mobility, and further open a route for the discovery of electronic sensors.

Naphthalene diimide (NDI)-based organic semiconductors have achieved great progress in high mobility and good air stability due to its delocalization structure and deep LUMO energy level. Herein, we performed a systematic investigation on the asymmetric side-chain dependent molecular packing and sensing performance with NDI derivatives. These semiconductors possess identical branched *N*-alkyl chains of $C_{10,12}$ on one side to increase the solubility and induced well-ordered assemblies. To obtain the asymmetric semiconductors, different linear alkyl chains containing conjugated benzene and non-conjugated alkyl chains on the other side were synthesized, which are named NDI-PhCn (n = 0, 2, 4, 6, 8, 12). Bottom-gate bottom-contact (BGBC) and bottom-gate top-contact (BGTC) devices were fabricated *via* spin-coating methods. The devices characteristics annealed at different temperature were summarized in Fig. S1 (Supporting information). The collected data clearly demonstrated the temperature dependence of device performance of OTFTs with different organic active layers. NDI-PhC0 and NDI-PhC2 shared similar mobilities in the range of 1.6 × 10^{-2} ~ 1.9 × 10^{-2} cm^2 V^{-1} s^{-1}, and I_{on}/I_{off} of 10^4. However, the device performance decreased sharply after annealing at high temperature. In order to keep the optimized signal amplification capabilities during gas sensing, the optimized annealing temperature for NDI-PhC0 is 160 °C, while it is 80 °C for other NDI derivatives were used in the following studies.

To understand the asymmetric side chain effect on electric characteristics of NDI-PhCns, we performed systematic investigation of OTFTs annealed at the optimized temperature (Table S1 in Supporting information). As shown in Fig. 1b and Fig. S2 (Supporting information), all the devices exhibited well-defined linear and saturation regions, with low contact resistance and hysteresis characteristics. Slightly higher mobilities were obtained in case of the BGTC devices owing to better carrier injection at the contact region. Clearly, NDI-PhC0, NDI-PhC2 and NDI-PhC12 shared similar mobilities in the range of 5.7 × 10^{-2} to 7.0 × 10^{-2} cm^2 V^{-1} s^{-1}, and I_{on}/I_{off} of over 10^4. With reducing the asymmetric degree by *n*-butane substitution, NDI-PhC4 yielded a mobility of 1.6 × 10^{-2} cm^2 V^{-1} s^{-1}. In contrast, NDI-PhC6 and NDI-PhC8 exhibited a maximum mobility of 2.9 × 10^{-3} and 4.9 × 10^{-4} cm^2 V^{-1} s^{-1} respectively, which are one and two orders of magnitude lower than the highest value achieved in case of NDI-PhC2 OTFTs. Moreover, a similar tendency of asymmetry-dependent mobility was observed for NDI-PhCn-based OTFTs with both BGBC and BGTC architectures. In this case, the mobilities first decreased and then increased, accompanied by a decrease in the degree of asymmetry (Fig. 1c).

Atomic force microscopy (AFM) was performed to explore the micro morphologies of the organic semiconductor films annealed under optimized temperature. NDI-PhCn films preferred an ordered, terraced surface microstructure after annealing (Fig. S3 in Supporting information), which was consistent with our previous study [27–29]. Fig. 2a summarized the AFM images of the optimized NDI-PhCn films, in which NDI-PhC0, NDI-PhC2 and NDI-PhC4 showed apparent terraced surface microstructure, and the

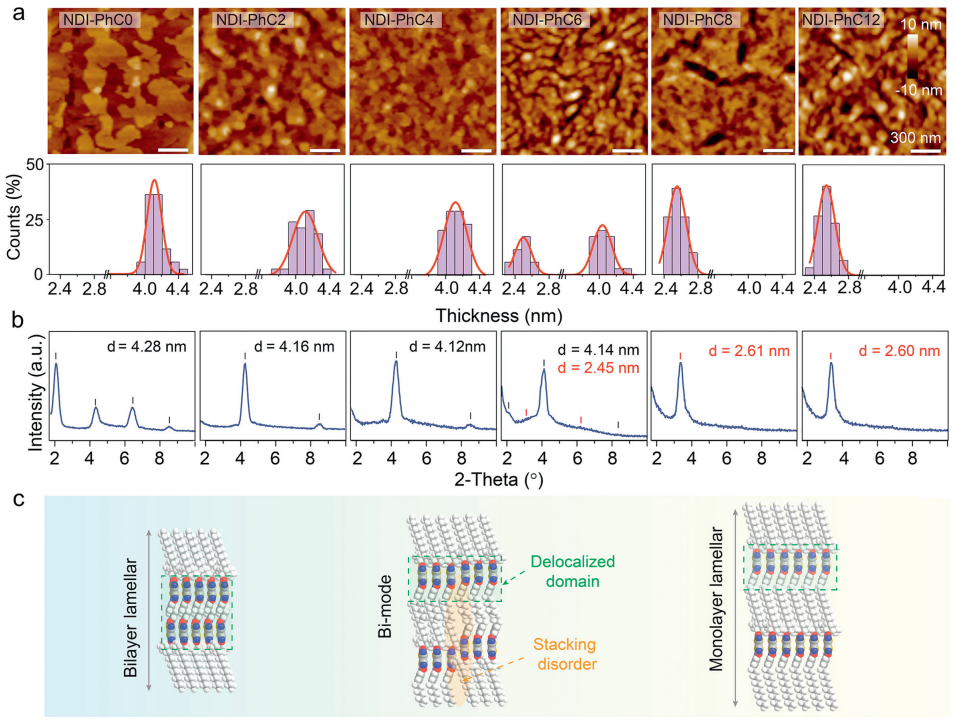

Fig. 2. (a) AFM images and corresponding thickness profile of the terrace structure, and (b) XRD patterns of NDI-PhC0, NDI-PhC2, NDI-PhC4, NDI-PhC6, NDI-PhC8, and NDI-PhC12 after thermal annealing at the optimized temperature. The black and red line present different diffraction sets. (c) Schematic of molecular packing of a head-to-head bilayer, bi-mode and a head-to-tail monolayer mode, respectively.

domain size decreased from 2.1 × 10^5 nm^2 to 1.2 × 10^5 nm^2, with increase in the side-chain symmetry. Further, the cross-section analysis of the AFM images demonstrated surface steps with a height of 4.19, 4.13, and 4.01 nm for NDI-PhC0, NDI-PhC2 and NDI-PhC4, respectively. A significant film microstructure change was observed when increasing the symmetry to NDI-PhC6, bearing one-branched N-alkyl chain of $C_{10,12}$ (14 carbon atoms in length) and a benzene alkyl chain of linear C6 (6 carbon atoms). Consequently, two obvious changes in the surface morphology were observed: (1) large pinholes and grain boundaries, and (2) two different surface steps, including 4.00 and 2.32 nm (simultaneously observed). However, this multiple molecular stacking may result in considerable number of trap densities, which may significantly hinder the carrier transport in the conductive channel. Moreover, the grain boundary was further enlarged in case of the NDI-PhC8 film, which resulted in the lowest carrier mobility. Whereas, the NDI-PhC8 and NDI-PhC12 films exhibited only one constant layer step, which was reduced to ~2.60 nm. It should be noted that the change of height analysis of surface steps in the terraced structure, which did not exhibit the same tendency as the length of the single molecule with increased value (Fig. S4 in Supporting information), indicated the importance of asymmetric side-chain engineering in molecular stacking and electric performance.

X-ray diffraction (XRD) measurements were further performed to test the intermolecular stacking of the NDI-PhCn molecules under thermal annealing (Fig. 2b). The sharp Bragg reflections of NDI-PhCn derivatives suggested a high degree of crystallinity in case of these small molecules. As calculated using Bragg's Law, d-spacing of NDI-PhCn were calculated to show the length of repeated layer-by-layer unit. The NDI-PhC0 film exhibited a d-spacing distance of 4.28 nm, which is consistent with the height of one terrace layer. Here, we further measured the angle-resolved NEXAFS spectroscopy of NDI-PhC0 to obtain information regarding molecular orientation of the conjugated backbone with respect to the plane of the substrate. As shown in Fig. S5 (Supporting information), the average title angles of the transition dipole moments (TDM) was 81.3° ± 0.5°, indicating that the molecules preferred an edge-on stacking orientation. Interestingly, the d-spacing distance was two times larger than the length of one single molecule (Fig. S4), indicating a bilayer molecular packing of NDI-PhC0 standing on the substrate after annealing at 160 °C. According to UV-spectra (Fig. S6 in Supporting information), NDI-PhC0 exhibited a bathochromic-shifted 0–1 peak because of *J*-aggregation along the π-backbones [30,31]. For NDI-PhC2 and NDI-PhC4, we speculated that the molecules preferred a bilayer stacking mode, as indicated by the uniform height of surface steps at ~4.20 nm and large d-spacing of ~4.15 nm. The first diffraction peak at 2.07° was not probed, which may be caused by a lower degree of crystallinity in NDI-PhC2 and NDI-PhC4. In comparation, NDI-PhC8 and NDI-PhC12 films with lower asymmetry degree exhibited a d-spacing distance of ~2.6 nm, comparable to one molecular layer. Corresponding UV-spectra also exhibited an intensity ratio of 0–0 to 0–1 peak over 1, indicating a *J*-aggregation because of stronger π-π coupling. Moreover, there were two sets of diffraction peaks for NDI-PhC6 film with crystalline d-spacing distance of 4.14 and 2.45 nm, respectively, thus indicating the dominate molecular packing changes from bilayer to monolayer style.

Considering the above results and previous publications, we described the molecular stacking models for NDI-PhCn derivatives in Fig. 2c: (1) NDI-PhCns with high asymmetric alky-chain substitution preferred a head-to-head lamellar assembly; (2) with decrease in the degree of asymmetry, the molecular stacking became more random and complex; (3) a head-to-tail monolayer lamellar assembly was dominant after substituting with a symmetric side chain. As expected, the interactions between NDI-PhCns along the out of plane direction considerably influenced the molecular stacking. Hence, charge transfer integral was calculated through density function theory (DFT) calculations using the Gaussian 09 program with B3LYP/6–31G* functionals with a D3 dispersion correction [32–36]. As the molecular coupling along the *J*-aggregation

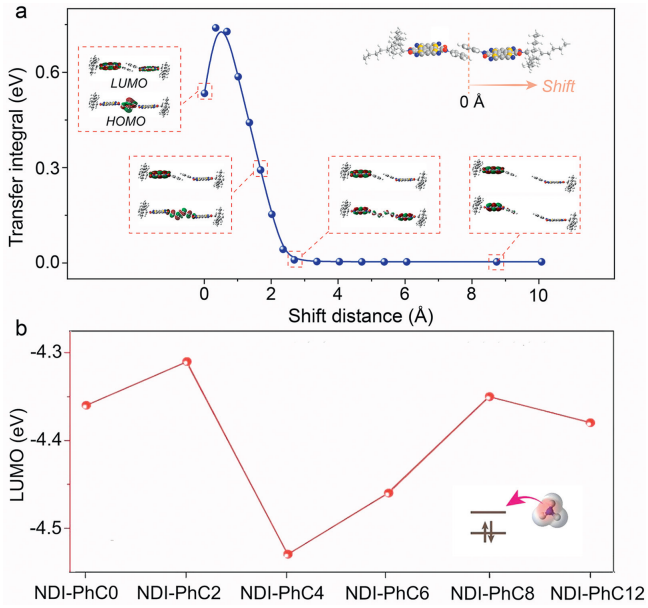

Fig. 3. Molecular packing modal and corresponding interaction: (a) Dependency of the transfer integral on the shift distance of NDI-PhC0 dimer. (b) LUMO energy level of NDI-based thin films measured through LEIPS.

directly contribute to the head-to-head/tail assembly, we simplified the transfer integrals analysis to the adjacent σ-π NDI-PhC0 pairs. In this case, a dense packed NDI-PhC0 bilayer was speculated based on d-spacing and transition dipole moments which set as the input configuration without molecular displacement. When molecules packed with a head-to-head model, the distance of conjugated core would increase with increasing the linear alkyl chains. Hence, we enlarged the distance between two NDI-PhC0 to simulate the linear-alkyl chains substitution.

As shown in Fig. 3a, the charge transfer integral was estimated from 529 meV to a maximum of 734 meV when the distance between the two molecules reached 0.54 Å. This value is similar to the reference transfer integral for the adjacent π-π pair of NDI derivatives [37], owing to the Vans der Waals interaction between the phenyl groups. This result contributes to efficient molecular coupling in two directions, yielding a bilayer motif with large π-delocalized domain for high carrier mobility (Fig. 2c). A further increase in the shift distance decreased the charge transfer integrals along σ-π direction, which then disappeared at a value >2.8 Å. The distance of the transit point was equal to the length of a linear phenyl-alkyl chain with 6–8 carbon atoms. Thus, we proposed that the symmetric side chain engineering weakened the intermolecular force of the phenyl group and subsequently disturbed the packing orientation. Consequently, a head-to-head and head-to-tail bimodal packing was induced for NDI-PhC6. The multiple molecular packing somehow induced a disorder microstructure and increased grain boundary, which significantly hampered the carrier transport. With increase in the length of the linear alkyl chain, NDI-PhC8 and NDI-PhC12 became an almost symmetrical molecular, thus, tend to be packed as the head-to-tail modal with anisotropic molecular interactions. For NDI-PhC12, the film could exhibit an ordered edge-on stacking owing to the side-chain-interdigitation assisted molecular assembly, in turn yielding a higher carrier mobility. These results clearly demonstrate that the asymmetric degree of substituted alkyl-chain can manipulate molecular stacking and carrier transport by trading off adjacent molecular interactions. Another compelling evidence is the red shift of UV absorption at 0–0 and 0–1 and the change of 0–0/0–1 intensity ratio of NDI-PhCns with increased asymmetry, verifying the decreased π-conjugation delocalization (Fig. S6b in Supporting information and Fig. 3a). However, it also should be noticed that if the *J*-aggregation along σ-π direction becomes tight, although the intermolecular force can be strengthened, it will also induce a vertical displacement of adjacent conjugated cores and large steric hindrance which paid off the molecular coupling effect [27,38].

As the delocalization is closely related to the molecular orbitals energy, we revealed electric structure of NDI-PhCns [39,40], combined with DFT, cyclic voltammetry (CV), ultraviolet photoelectron spectroscopy (UPS) and low-energy inverse photoemission spectroscopy (LEIPS) (Figs. S7-S9 in Supporting information). The highest occupied molecular orbital (HOMO) and lowest unoccupied molecular orbital (LUMO) of NDI-PhCns in the liquid and solid states were summarized in Table 1. Interestingly, we found that the LUMO level of NDI-PhCns calculated from DFT in solid and CV method were nearly identical, because of the non-aggregated features. However, the LUMO level changed significantly for solid NDI-PhCn (Fig. 3b). The film of NDI-PhC0 and NDI-PhC2 with a head-to-head bilayer stacking, exhibited a LUMO level of −4.36 and −4.31 eV respectively, due to higher degree of delocalized structures owing to the coupling of conjugated cores. In contrast, NDI-PhC4 possessed the deepest LUMO level down to −4.53 eV owing to smaller steric hindrance compare to NDI-PhC0 and NDI-PhC2. The result coordinated to molecular asymmetric degree can be attributed to molecular displacement enhanced transfer integrals along π-π direction, resulting in a deeper LUMO. When the molecular stacking model transits from bilayer to monolayer case, the LUMO level in turn increase to −4.38 eV related to the variation tendency of electronic coupling. Although the electric structure is not directly related to the electron transport mobility, it can officially reflect the charge-transfer activity response to external analytes films. Based on a simulation, larger energy changes (ΔE) were estimated for the chemical interaction between ammonia with bilayer stacking NDI-PhCn dimers (Fig. S10 in Supporting information). Simultaneously, NDI-PhC4 yielded the deepest LUMO level of −4.53 eV, which contributed to the strongest electron accepting capacity which are expected with the strongest electron affinity to ammonia (Fig. S10).

To systematically study the asymmetric substitution effect on gas sensing, we conducted real-time ammonia detection based on NDI-PhCn transistors with BGTC geometry. Ammonia is a biomarker of renal failure and liver disease, which is in the range of 500–2100 ppb in the breath of healthy people [41]. It frequently works as an electron donor, which can donate electrons to the NDI-based derivatives through charge transfer reaction. Fig. 4a shows the dynamic sensing performance of NDI-PhCn based sensor for ammonia gas. Notably, the device performance kept constant after long-term storage (Fig. S11 in Supporting information), which is ideal for sensing applications. The device sensitivity to ammonia is calculated as $\Delta I/I_0 = (I_t\text{-}I_0)/I_0$, where I_t and I_0 are the source-drain current after and before exposure to the ammonia gas, respectively, and ΔI is the current change. Importantly, we obtained rapid and sensitive current response to ammonia, exhibiting a linear calibration curve between $\Delta I/I_0$ and concentration in a large range. Importantly, the devices based on NDI-PhC4 exhibited a $\Delta I/I_0$ up to 150% to 0.01 ppb ammonia, which is four orders of magnitude higher that the devices based on NDI-PhC0, NDI-PhC6, NDI-PhC8 and NDI-PhC12 (Fig. 4b). To the best of our knowledge, NDI-PhC4 achieved the highest sensitivity to ammonia gas in OFET-based ammonia gas sensors till date (Fig. 4c, Table S2 in Supporting information).

The question that arises is the mechanism by which the asymmetric alkyl-chain substitution manipulates the sensitivity to gasses. We hypothesize that molecular structure dependent electric structure originally tunes the sensing performance by trading off the chemical reactivity of the active layer, device amplification

Table 1
Summarized parameters of NDI-PhCn semiconductors measured in solution and thin film case.

Organic semiconductor	Solution				Film	
	E_{Red} (V)[a]	E_{LUMO}(eV)[b]	E_{HOMO} (eV)[c]	E_g (eV)[d]	E_{LUMO} (eV)[e]	E_{HOMO} (eV)[f]
NDI-PhC0	0.105	−4.38	−6.42	2.04	−4.36	−7.09
NDI-PhC2	0.147	−4.42	−6.49	2.07	−4.31	−6.95
NDI-PhC4	0.141	−4.41	−6.47	2.06	−4.53	−6.97
NDI-PhC6	0.109	−4.38	−6.43	2.05	−4.46	−7.04
NDI-PhC8	0.121	−4.39	−6.44	2.05	−4.35	−7.01
NDI-PhC12	0.118	−4.39	−6.44	2.05	−4.38	−7.08

[a] Estimated from electrochemical determination *versus* Fc/Fc^+.
[b] $E_{LUMO} = -(4.80 - E_{1/2,\ Fc/Fc^+} + E_{Red})$, assuming the absolute energy level of Fc/Fc^+ to be 4.8 eV below vacuum.
[c] $E_{HOMO} = E_{LUMO} - E_g$.
[d] Estimated from the adsorption edge of the UV adsorption spectra.
[e] Calculated from LEIPS of the thin film.
[f] Calculated from UPS of the thin film.

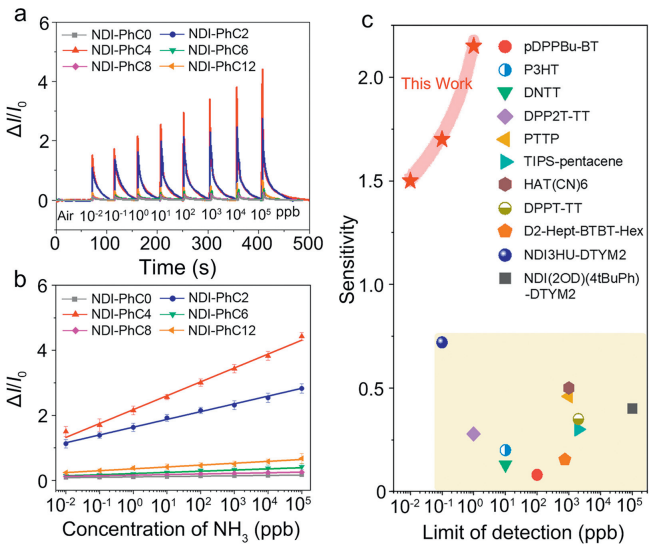

Fig. 4. (a) Current responses of NDI-PhCn based gas sensor to a series of ammonia concentrations. The real-time current response is calculated by the percent change in current ΔI with respect to the initial current I_0. (b) Read-out $\Delta I/I_0$ of NDI-PhCn devices to ammonia with concentration ranging 0.01 ppb to 100 ppm (v/v). (c) The limit of detection and sensitivity of bilayer stacking NDI-PhCn devices in comparison with reported sensors.

and gas diffusion pathways (Fig. 5a). The direct signal transition originates based on the LUMO level, as discussed above, for the chemical activity between the analyte and the conductive channel.

To quantify the extent to which the charge transfer reaction modulated by molecular structure, we performed fluorescent detection for NDI-PhCn films exposed to ammonia. As shown in Fig. S12 (Supporting information), all NDI-PhCn films exhibited a decreased fluorescent intensity under 540 nm when been examined under ammonia atmosphere, which was caused by the lone pair electrons of ammonia fulfilled the empty orbitals which prevented the excited molecules returning to the ground state [42]. The sensing discrimination defined as $\delta_{(\Delta I/I0)}/\delta_{concentration}$, where $\delta_{(\Delta I/I0)}$ and $\delta_{concentration}$ represent the sensitivity change at corresponding concentration variation, is extracted. Notably, the variation of normalized fluorescence intensity $(F\text{-}F_0)/F_0$ for NDI-PhCn derivatives was consistent with $\delta_{(\Delta I/I0)}/\delta_{concentration}$) with respect to the asymmetric substitution (Fig. 5b). These results verify that the interaction strength between ammonia and semiconductors with optimized chemical reactivity should be the main factor for ultrasensitive detection.

Further, the performance of OFET-based gas sensors is also related to the macroscopic properties, such as crystalline characteristics and film morphology, and microscopic properties such as molecular orientation, d-spacing and packing defects. Compared with NDI-PhC0 and NDI-PhC2, the crystal domain size of

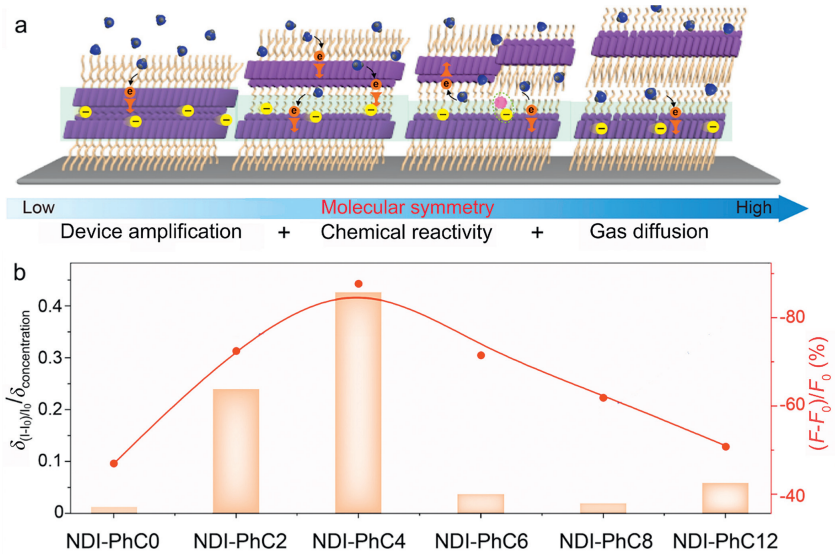

Fig. 5. (a) Schematic illustration of molecular asymmetry dependent bilayer-to-monolayer molecular stacking variation and sensing process. (b) The sensing discrimination $(\delta_{(\Delta I/I0)}/\delta_{concentration})$ of OTFTs and variation of normalized fluorescence intensity $((F\text{-}F_0)/F_0)$ of NDI-PhCn thin films after exposure to ammonia vapors.

NDI-PhC4 was smaller, thus facilitating gas diffusion through the grain boundary. Although the pinholes in NDI-PhC6 and NDI-PhC8 were beneficial for the sensitive response, the low mobility and high subthreshold swing limited the signal amplification ability of OTFTs. Hence, OTFTs based on NDI-PhC4 film obtained the highest sensitivity, suggesting the necessity of maintaining a balance between the electric LUMO level and device amplification ability. This observation clearly demonstrates the critical role of asymmetric side-chain engineering in chemical detection and contributes to a deeper understanding of the relationship between the molecular structure and sensitivity.

In summary, we conducted a systematic study on the carrier transport and charge transfer properties of six NDI derivatives with different asymmetric side chains. A combination of detailed thin-film characterization and theoretical calculation revealed that the molecular packing structures may change from head-to-head bilayer model to head-to-tail monolayer model. Notably, a tiny asymmetry decrease of NDI-PhCn derivatives results a unique 0.17 eV shift of LUMO level, which contributes to significant enhancement of chemical reactivity with Lewis base gas, subsequently, manipulating the charge transfer and sensitivity. Combined with high amplification abilities of OTFT device and comparatively more gas diffusion pathways, NDI-PhC4 achieved 150% current response even at low ammonia concentration of 0.01 ppb, which is approximately two times larger than that previously reported. All of the results demonstrated the critical role of asymmetric side chain in determining the molecular stacking and charge transfer process and provided more opportunities in fabricating highly sensitive and responsive chemical sensors. We believe that further optimization of organic semiconductor in both side chain asymmetric feature and functional group substitution, to achieve a larger energy level manipulation, may contribute to OTFT biosensors for selective detection.

Declaration of competing interest

The authors declare that they have no known competing financial interests or personal relationships that could have appeared to influence the work reported in this paper.

Acknowledgments

This research was financially supported by the National Natural Science Foundation of China (Nos. 6197396, 21905276), Natural Science Foundation of Beijing (No. 4202077), Chinese Academy of Scinece (No. ZDBS-LY-SLH034) and the Fundamental Research Funds for the Central Universities (No. E2ET0309X2). The authors also thank Prof. Christopher R. McNeill from Monash University, for facilitating the NEXAFS measurement.

Supplementary materials

Supplementary material associated with this article can be found, in the online version, at doi:10.1016/j.cclet.2023.108734.

References

[1] C.A. Di, H.G. Shen, F.J. Zhang, D.B. Zhu, Acc. Chem. Res. 52 (2019) 1113–1124.
[2] J.R. Sempionatto, R.K. Mishra, A. Martin, et al., ACS Sens. 2 (2017) 1531–1538.
[3] P. Kafle, F.J. Zhang, N.B. Schorr, et al., Adv. Funct. Mater. 30 (2020) 1909787.
[4] Y. Zhao, W. Wang, Z. He, et al., Chin. Chem. Lett. 27 (2022) 108094.
[5] A. Tsumura, H. Koezuka, T. Ando, Appl. Phys. Lett. 49 (1986) 1210–1212.
[6] B. Peng, S. Huang, Z. Zhou, P.K.L. Chan, Adv. Funct. Mater. 27 (2017) 1700999.
[7] C. Song, J. Yun, H. Lee, et al., Adv. Funct. Mater. 29 (2019) 1901996.
[8] D. Zhi, E. Zhang, B. Zhang, F. Zhang, Mol. Syst. Des. Eng. 7 (2022) 553–568.
[9] S. Yang, X. Zhang, P. Chen, et al., Adv. Electron. Mater. 3 (2017) 1700120.
[10] L. Torsi, G.M. Farinola, F. Marinelli, et al., Nat. Mater. 7 (2008) 412–417.
[11] Y. Wang, Q. Gong, Q. Miao, Mater. Chem. Front. 4 (2020) 3505–3520.
[12] S. Fratini, M. Nikolka, A. Salleo, G. Schweicher, H. Sirringhaus, Nat. Mater. 19 (2020) 491–502.
[13] H. Bronstein, C.B. Nielsen, B.C. Schroeder, I. McCulloch, Nat. Rev. Chem. 4 (2020) 66–77.
[14] R.A. Soomro, S. Jawaid, Q. Zhu, Z. Abbas, B. Xu, Chin. Chem. Lett. 31 (2020) 922–930.
[15] X.Y. Ma, Z.L. Jiang, L.Y. Xiang, F.J. Zhang, ACS Mater. Lett. 4 (2022) 918–937.
[16] K.S. Park, J.J. Kwok, P. Kafle, Y. Diao, Chem. Mater. 33 (2021) 469–498.
[17] S.W. Yun, J.H. Kim, S. Shin, et al., Adv. Mater. 24 (2012) 911–915.
[18] F.J. Zhang, G. Qu, E. Mohammadi, J. Mei, Y. Diao, Adv. Funct. Mater. 27 (2017) 1701117.
[19] J. Lu, D. Liu, J. Zhou, et al., Adv. Funct. Mater. 27 (2017) 1700018.
[20] Q. Gong, Q. Miao, Chem. Commun. 58 (2022) 7046–7049.
[21] F.J. Zhang, V. Lemaur, W. Choi, et al., Nat. Commun. 10 (2019) 4217.
[22] B.M. Oh, S.H. Park, J.H. Lee, et al., Adv. Funct. Mater. 31 (2021) 2101981.
[23] Y. Yang, G. Zhang, H. Luo, et al., ACS Appl. Mater. Inter. 8 (2016) 3635–3643.
[24] H. Iino, T. Usui, J. Hanna, Nat. Commun. 6 (2015) 6828.
[25] T. Mori, T. Yasuda, Adv. Electron. Mater. 7 (2021) 2001052.
[26] S. Arai, K. Morita, J.Y. Tsutsumi, et al., Adv. Funct. Mater. 30 (2019) 1906406.
[27] F.J. Zhang, Y. Hu, T. Schuettfort, et al., J. Am. Chem. Soc. 135 (2013) 2338–2349.
[28] F.J. Zhang, C.A. Di, N. Berdunov, et al., Adv. Mater. 25 (2013) 1401–1407.
[29] Y.P. Zang, F.J. Zhang, D.Z. Huang, et al., Adv. Mater. 26 (2014) 2862–2867.
[30] M. Li, H. Bin, X. Jiao, et al., Angew. Chem. Int. Ed. 59 (2020) 846–852.
[31] H. Kar, D.W. Gehrig, N.K. Allampally, et al., Chem. Sci. 7 (2016) 1115–1120.
[32] Y. Jin, J.A. Qiao, C. Liu, et al., J. Phys. Chem. C 123 (2019) 20093–20104.
[33] M. Yoneya, J. Phys. Chem. C 122 (2018) 22225–22231.
[34] S.N. Afraj, C. Lin, A. Velusamy, et al., Adv. Funct. Mater. 32 (2022) 2200880.
[35] M.J. Frisch, G.W. Trucks, H.B. Schlegel, et al., Gaussian 09, Revision A.01, Gaussian, Inc., Wallingford, CT, 2009.
[36] S. Grimme, J. Antony, S. Ehrlich, H. Krieg, J. Chem. Phys. 132 (2010) 154104.
[37] T. Okamoto, S. Kumagai, E. Fukuzaki, et al., Sci. Adv. 6 (2020) eaaz0632.
[38] H. Chung, S. Chen, B. Patel, et al., Cryst. Growth Des. 20 (2020) 1646–1654.
[39] S. Duhm, G. Heimel, I. Salzmann, et al., Nat. Mater. 7 (2008) 326–332.
[40] R.Joseph Kline, M.D. McGehee, M.F. Toney, Nat. Mater. 5 (2006) 222–228.
[41] L. Andre, N. Desbois, C.P. Gros, S. Brandes, Dalton Trans. 49 (2020) 15161–15170.
[42] H. Li, Y. Shi, G. Han, et al., Angew. Chem. Int. Ed. 59 (2020) 4380–4384.